PERSPECTIVE • OPEN ACCESS

Time-resolved optothermal techniques to track the spatiotemporal evolution of temperature

Journal of Physics: Materials

OPEN ACCESS

RECEIVED
27 March 2026

REVISED
25 August 2026

ACCEPTED FOR PUBLICATION
28 August 2026

PUBLISHED
8 September 2026

PERSPECTIVE

Time-resolved optothermal techniques to track the spatiotemporal evolution of temperature

Loïc Moczko[1,3], Sebin Varghese[1,3], Nupur V Sontakkey[1], René J A Bruikman[1], Bas van Dijck[1], Max van Hemert[1], David Saleta Reig[2], Hugh Ramsden[1], Bohai Liu[1] and Klaas-Jan Tielrooij[1,2,*]

[1] Department of Applied Physics and Science Education, Eindhoven University of Technology, Den Dolech 2, Eindhoven 5612 AZ, The Netherlands
[2] Catalan Institute of Nanoscience and Nanotechnology (ICN2), CSIC and BIST, Campus UAB, Bellaterra, Barcelona 08193, Spain
[3] These authors contributed equally.
[*] Author to whom any correspondence should be addressed.

E-mail: k.j.tielrooij@tue.nl

Keywords: thermal transport, time-resolved techniques, thermal properties, optothermal microscopy

Supplementary material for this article is available online

Abstract

The ability to understand, control, and engineer heat flow is central to applications ranging from energy conversion to thermal management. Heat transport is particularly interesting at the micro- and nanoscale, where the conventional description of diffusive heat conduction can break down and where interfacial thermal transport becomes increasingly relevant. Probing nanoscale heat transport requires experimental methods that are non-invasive, compatible with ultrathin samples, and capable of resolving heat dynamics across interfaces between different materials. Optical pump-probe techniques provide a powerful contactless solution, combining high spatial and temporal resolution to accurately map the temporal dynamics and spatial evolution of material temperatures. Here, we first discuss the recently established technique of spatiotemporal thermometry (STT), which is particularly suitable for in-plane thermal transport. We then propose the technique of material-selective time-resolved thermometry, which is particularly suitable for out-of-plane heat transport. Both techniques follow the evolution of the temperature of thin films in time and space. Together, these two time-resolved approaches provide a platform for quantifying heat transport parameters in materials down to atomic thicknesses, with great potential for exploring nanoscale thermal phenomena.

1. Introduction

The thermal properties of a material govern its ability to dissipate excess energy in devices [1], determine its role in thermal management strategies [2] and dictate the efficiency of energy conversion in thermoelectric systems [3]. Poor heat dissipation can limit device lifetime and performance, while controlled heat flow enables enhanced performance. Understanding how heat flows through materials is therefore central to both technological development and the fundamental study of nanoscale systems [4]. It is particularly interesting to study heat transport at reduced length scales, on the order of the mean free path of heat-carrying phonons, where (quasi-)ballistic [5–9] and hydrodynamic [10–15] transport phenomena can occur. Another important aspect of nanoscale heat transport is thermal conduction across material interfaces, where phonon transmission is governed by vibrational mismatch and interfacial coupling, which are characterized by the thermal boundary conductance (TBC), or inversely, the Kapitza resistance [16].

After decades of progress, the experimental study of heat transport is now a well-developed field that benefits from a broad range of established techniques. Among these, electrical methods such as AC calorimetry [17], the 3ω technique [18], and microheater-based approaches [19] have allowed accurate measurements of the thermal properties of many materials and miniaturized systems [4, 20]. However,

their implementation often requires direct electrical contacts [21] and/or potentially complex device fabrication processes. In addition, these techniques offer limited spatial resolution and do not provide time-resolved information. Optothermal methods provide certain advantages, as they are based on contact-free, temperature-sensitive optical measurement approaches. Raman thermometry, for example, can be used to determine the thermal conductivity by locally heating a sample and monitoring temperature-dependent changes in the Raman response—such as peak shifts, linewidth variations, and Stokes/anti-Stokes intensity ratios. This technique can also be used to investigate interfacial heat transport [22]. In frequency-domain thermoreflectance (FDTR), a modulated heating laser induces reflectivity changes on a metal transducer deposited over the material(s) of interest, and a probe laser evaluates these changes as a function of the heating frequency, which in turn depends on the thermal properties of the materials underneath the metal transducer [23]. In an analogous way, time-domain thermoreflectance (TDTR) [24–26] uses pulsed lasers to track the temporal heat dynamics of such metallic transducers, from which the thermal properties of the underlying material(s) can be determined. Another time-resolved approach is transient thermal grating (TTG) thermometry, where two overlapped pump beams generate a spatially periodic temperature profile, and a probe beam experiences diffraction that varies as a function of pump-probe delay time, as heat diffuses [27, 28]. These optothermal techniques have established themselves as powerful and well-established methods to measure heat transport and thermal properties of a broad range of materials, despite often relying on complex mathematical modeling and, in some cases, requiring strong local heating.

Here, we discuss two time-resolved, all-optical techniques that enable quantitative studies of thermal transport in thin films, with nanometer accuracy and sub-picosecond time resolution. First, in section 1, we describe spatiotemporal thermometry (STT), which enables studying *in-plane* heat diffusion by tracking in time the broadening of spatial profiles that are related to temperature profiles. Second, in section 2, we introduce a time-resolved technique to investigate *out-of-plane* thermal transport, namely material-selective time-resolved (MaSTR) thermometry. This technique monitors the temperature evolution of individual slabs of a multilayer structure through temperature-dependent resonant modes. Together, these techniques provide an all-optical, contact-free platform for extracting thermal transport properties, in particular the in-plane thermal conductivity, the out-of-plane thermal conductivity, the interfacial thermal (Kapitza) resistances, and the heat capacity. Whereas we will highlight the capabilities of these techniques by providing examples based on two-dimensional materials, the techniques and methodologies are broadly applicable to a wide range of thin-film and multilayer systems, beyond two-dimensional materials. Our goal is to offer both conceptual context and practical guidance for using these two time-resolved optical methods to study thermal transport.

2. Spatiotemporal thermometry (STT)

2.1. The concept of STT

The concept of STT is the following (see figure 1(a)): a pump pulse photoexcites a material, either by leading directly to lattice heating or indirectly through electronic excitations that transfer energy to the lattice. The rate at which an excitation is transferred to the material as heat depends on the properties of the material(s) of interest, in particular the electron and phonon relaxation times. The presence of lattice heat changes the optical properties of the material, which is detected as a change in reflection of a probe pulse that arrives with a variable time delay compared to the pump pulse. Spatially scanning the probe across the pump spot at different pump–probe delays results in maps that reflect the spatiotemporal evolution of the heat distribution, thus revealing how heat spreads in the material and enabling the extraction of thermal transport properties. Probing this heat around specific temperature-dependent resonances, such as excitons or plasmons, leads to the strongest optothermal response and therefore the highest sensitivity to temperature changes. This is not strictly necessary, since the reflectance away from resonances is typically also (weakly) temperature dependent. Ideally, one should operate this technique in a regime where the change in reflection is linear in incident power and therefore linear in temperature, because this ensures that the transient reflection profile represents a temperature profile.

The STT technique has in common with TTG that it is sensitive to heat transport with both spatial and temporal resolution. Although the pump-probe scheme is similar to that of TDTR measurements, the STT technique does not require a transducer. Thermal properties are inferred from the evolution of the excitation response instead of absolute temperature measurements, eliminating the need to know how much power has been absorbed from pump excitation to obtain the absolute temperature of the material. In terms of samples, it typically simply requires a uniform thin film of a material of interest. In

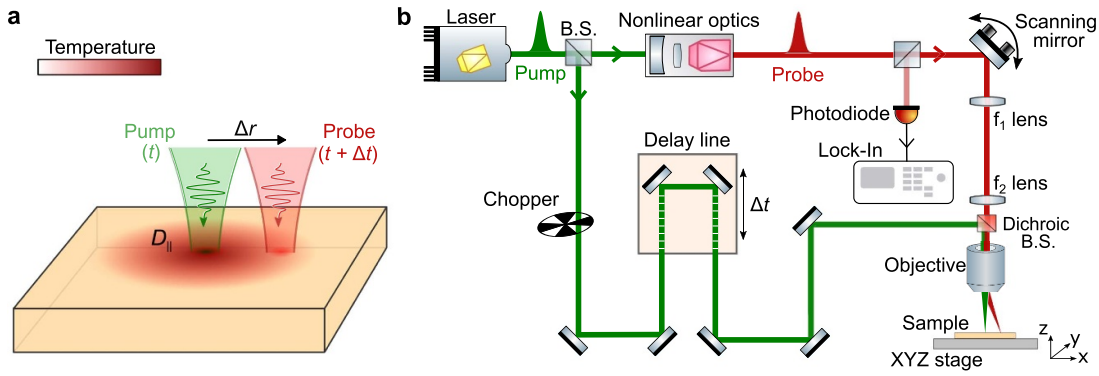

Figure 1. Concept and experimental implementation of spatiotemporal thermometry. (a) Pump pulses (green) create a local hotspot in a material of interest. Probe pulses (red) scan across the pump spot at varying time delays Δt to measure the evolving temperature distribution, enabling the tracking of temperature in space and time. (b) Schematic of a spatiotemporal thermometry setup. A scanning mirror steers the probe beam that is imaged onto the back aperture of the objective using a $4f$ relay formed by two lenses with focal lengths f_1 and f_2. In a conjugate configuration, angular deflections of the mirror translate into lateral displacements at the sample plane while maintaining the probe focus. B.S. is beam splitter.

some cases, it is necessary to suspend the material over a hole to minimize the effects of the substrate on heat transport.

2.2. Implementation of a STT setup

Figure 1(b) illustrates a possible implementation of an STT setup, where a laser source generates optical pump pulses that photoexcite the sample, which heats up. Probe pulses that are derived from the same laser source via a nonlinear optics stage, are sensitive to temperature-induced changes in transient reflectivity $\Delta R/R$. An optical delay line controls the temporal delay Δt between pump and probe pulses, and a scanning mirror controls the position of the focus of the probe pulse relative to the pump focus. This allows for mapping the temperature response as a function of the pump-probe offset Δr. The pump beam is modulated with a fixed frequency f_{mod} using a mechanical chopper, and a lock-in amplifier extracts the pump-induced change in reflectivity, i.e. the thermal response at the modulation frequency f_{mod}. The reflected probe light is separated from the reflected pump light using a dichroic beam splitter and detected by a photodiode. Recording the probe signal as a function of pump-probe offset Δr and delay time Δt allows the reconstruction of a two-dimensional map, or one-dimensional linecuts, of the local temperature response. Analysis of the broadening of spatial temperature profiles at different pump–probe delays provides direct access to in-plane thermal transport and enables the extraction of the in-plane thermal diffusivity $D_{\|}$.

Depending on the relaxation dynamics of a material relative to the laser repetition rate, two distinct regimes can occur: (i) a non-accumulating heat regime, in which the pump-induced temperature rise fully decays before the arrival of a subsequent pulse, such that each pump-induced excitation event is thermally independent; and (ii) an accumulating heat regime, in which the system does not fully relax between pulses, leading to residual heating and energy accumulation over multiple excitation cycles. Below, we explain for both regimes how to extract the in-plane thermal diffusivity $D_{\|}$.

2.3. Heat transport in the non-accumulating heat regime

We first consider the non-accumulating heat regime, where heat transport leads to a straightforward broadening of the spatial temperature profile as a function of pump-probe delay time. The experimental transient reflectivity profile at each pump–probe delay can be described by a Gaussian function:

$$\frac{\Delta R}{R}(\Delta r, \Delta t) = A(\Delta t) \exp\left[-\frac{\Delta r^2}{2\sigma^2(\Delta t)}\right], \tag{1}$$

where $A(\Delta t)$ is the amplitude of the relative reflectivity change and $\sigma(\Delta t)$ is the Gaussian width at delay Δt (see figure 2(a)). The diffusivity follows from the temporal evolution of the width:

$$D_{\|} = \frac{\sigma^2(\Delta t) - \sigma^2(0)}{2\Delta t}. \tag{2}$$

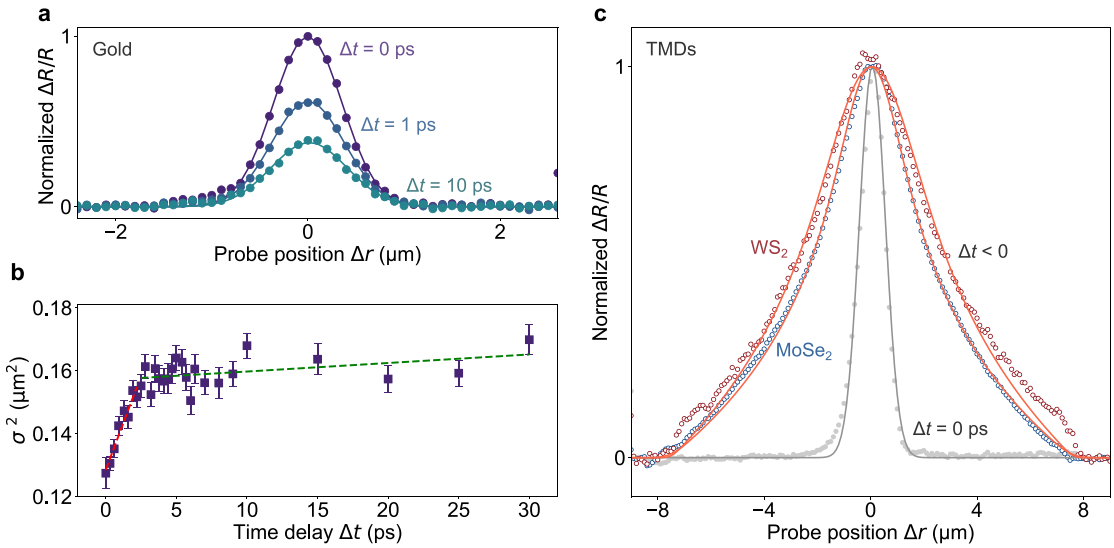

Figure 2. Obtaining heat transport properties using STT. (a) STT measurements on a thin gold film: transient reflectivity profiles (normalized to the $\Delta t = 0$ ps profile) at selected time delays, with a single Gaussian fit. (b) Temporal evolution of the Gaussian width squared (σ^2), showing fast electronic heat diffusion (≈ 60 cm^2 s^{-1}), followed by slower phononic heat diffusion (≈ 1.4 cm^2 s^{-1}) in the non-accumulating heat regime. Reprinted with permission from [32]. Copyright (2023) American Chemical Society. (c) Heat diffusion observed in suspended TMDs ($D_{\parallel} = 0.18$ cm^2 s^{-1} and 0.59 cm^2 s^{-1} for $MoSe_2$ and WS_2, respectively) in the accumulating heat regime. Reprinted from [36], with the permission of AIP Publishing.

This Gaussian-tracking approach can, in principle, capture both charge and phonon heat diffusion of a broad range of materials [29]. For example, Delor *et al* [30] employed this approach to measure the thermal diffusivity of silicon using spatiotemporal wide-field imaging, finding a value of 0.6 ± 0.2 cm^2 s^{-1}, corresponding to a thermal conductivity of approximately 100 W m^{-1} K^{-1}. Block and coworkers [31, 32] used STT to measure in-plane heat diffusion in gold, finding a thermal diffusivity of approximately 1.4 cm^2 s^{-1} in the regime where electrons and phonons are in thermal equilibrium (see figure 2(b)). Using the same technique, the thermal diffusivity of hBN-encapsulated MoS_2 [33], disordered gold films [34], and semiconductor nanocrystals [35] were determined.

2.4. Heat transport in the accumulating heat regime

The accumulation regime occurs when the thermal relaxation time of the material is comparable to, or longer than, the delay between sequential pulses [37]. In this case, the spatiotemporal temperature evolution during a modulation cycle is shaped by the cumulative contribution of multiple pulses. To model this regime and extract the in-plane thermal diffusivity, Fourier's diffusive heat equation is numerically simulated for a localized Gaussian heat source, as described in [36]:

$$\frac{\partial T}{\partial t} = D_{\parallel}\nabla^2 T + S, \tag{3}$$

where T is the lattice temperature, t is time, $D_{\parallel}$ is the diffusivity, ∇ is the multi-dimensional gradient, and S describes any source term. Successive pump pulses are added at intervals set by the laser repetition rate (f_{rep}) and modulation frequency (f_{mod}) with a total of $N = f_{\mathrm{rep}}/2f_{\mathrm{mod}}$ pulses per pump-on window for a 50% duty cycle. The resulting temperature dynamics are processed using a lock-in detection scheme to obtain the in-phase and out-of-phase spatial temperature profiles. These simulated profiles are compared to the experiment to determine the thermal diffusivity, after convolution with the probe beam profile to reproduce experimental conditions.

Applying this approach to two-dimensional semiconducting materials, the heat-accumulation regime has been used to investigate suspended TMD films via the temperature-dependent broadening of excitonic resonances [36]. By analyzing the $\Delta t < 0$ signal, [36] demonstrated the ability to access a steady-state residual lattice temperature profile that results from heat accumulation over multiple laser pulses in thin TMD flakes. The obtained in-plane thermal diffusivities were 0.18 cm^2 s^{-1} for $MoSe_2$, 0.20 cm^2 s^{-1} for WSe_2, 0.35 cm^2 s^{-1} for MoS_2, and 0.59 cm^2 s^{-1} for WS_2 (see figure 2(c)). By multiplying the measured diffusivities with the volumetric heat capacity C_v, they obtained the in-plane thermal conductivity $\kappa_{\parallel}$ of these films, in good agreement with values reported in the literature. [38].

2.5. Prospects and limitations of STT

The technique of STT offers several notable advantages. It is fully non-invasive and contact-free, and it provides two complementary routes to extract the in-plane thermal diffusivity of thin films: (i) by describing the spatial profile with a Gaussian function in the non-accumulating heat regime, or (ii) by comparing the measured profiles with a simple Fourier-based diffusion model in the accumulating heat regime. Importantly, neither approach requires material-specific parameters, which are often essential in other optothermal techniques. Another advantage of the technique is its high sensitivity. In TMDs, measurements indicate a thermoreflectance coefficient on the order of 10^{-4} K^{-1} [36], comparable to the maximum sensitivity achieved using gold transducers, while probing the temperature of the material of interest via excitons. As a result, a temperature rise smaller than 1 K produces a measurable transient reflectivity change, since pump-probe techniques can resolve transient reflectivity changes below 10^{-4}, highlighting the technique's ability to detect subtle thermal perturbations.

Although the examples given here were based on heat transport following Fourier's law, this technique is capable of revealing deviations from this law. In particular, it is possible that the shape of the temperature-dependent transient reflectivity profiles develops in a way that cannot be explained by Fourier's law. Manifestations of hydrodynamic heat transport, such as second sound, where heat transport shows wave-like behavior [39], will result in observable deviations in the profile evolution described in equation (1). Recently, non-Fourier heat transport, where thermoelastic and hydrodynamic effects together led to highly viscous heat transport, was indeed observed using this technique [40]. In some non-diffusive transport cases, the temperature evolution can be represented by an effective diffusivity, and it may depend on pump-spot size, pump modulation frequency, laser repetition rate, excitation wavelength, and optical penetration depth.

Despite these strengths, the method also comes with certain limitations. Materials with long-lived photoexcited carriers may be dominated by electronic diffusion contributions, complicating the extraction of the phonon heat diffusivity. An effective solution is the use of infrared pump pulses to directly excite lattice vibrations, suppressing electronic transport effects [41]. Furthermore, the 2D diffusion model assumes uniform out-of-plane heating, which holds when the film thickness is small compared to the lateral extent of the heated region and the optical penetration depth. For thicker samples or materials with extremely low out-of-plane thermal conductivity, a full 3D diffusion description becomes necessary.

Looking ahead, STT opens the door to probing physical processes that were previously difficult to access. Combining the thermal diffusivity extracted from this approach with an independent measurement of the thermal conductivity would enable the determination of the heat capacity of thin films. The technique also provides a powerful platform for exploring non-diffusive heat transport and for studying more complex structures such as van der Waals heterostructures, where material-specific resonances offer intrinsic layer selectivity. In addition, pulse-picking or variable-repetition-rate lasers can extend the flexibility of the method by increasing the spacing between pulses, thereby eliminating any negative-delay signal and enabling the use of simple Gaussian-width analysis (see section 2.3) to extract the in-plane thermal diffusivity. Together, these developments point to a broad and expanding landscape for future applications of this technique.

3. MaSTR thermometry

3.1. The concept of MaSTR thermometry

The concept of MaSTR thermometry, which is a technique that we introduce here, is to use pump pulses to heat a transducer material and then to follow the spreading of heat from the transducer into the material(s) below the transducer by directly probing the material(s). The timescale by which the excitation is transferred as heat into the material of interest, just like in TDTR, is determined by electron and phonon relaxation times, and thermal boundary resistances. By using time-delayed probe pulses that are sensitive to temperature-dependent and material-specific resonances, this enables observing heat transport through different materials in time. This transport is typically governed by the TBCs (or Kapitza resistances) and the out-of-plane thermal conductivity of the materials [16]. In this technique, the material(s) of interest is (are) placed on a substrate and coated with a metallic transducer (see figure 3(a)). The substrate should be transparent for the probe pulses, as this technique requires pumping the transducer from one side of the sample and probing the material(s) underneath the transducer from the other side. Under certain conditions, this technique enables a direct determination of the TBC and the out-of-plane thermal conductivity, as we will show.

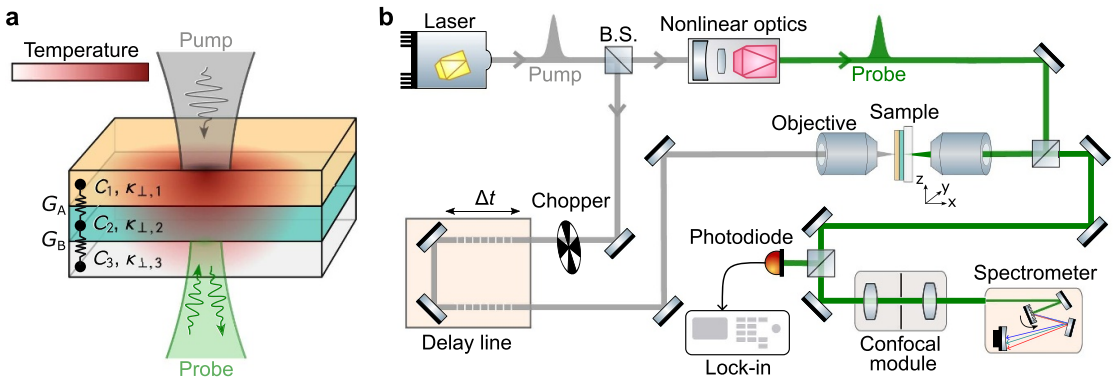

Figure 3. Concept and experimental implementation of material-selective time-resolved (MaSTR) thermometry. (a) Conceptual sketch of a typical sample formed of three layers. Layer 1 corresponds to the metallic transducer, layer 2 to the material of interest, and layer 3 to a transparent substrate. We label the interface between layers 1 and 2 as 'A' and the interface between layers 2 and 3 as 'B'. Heat transport in the out-of-plane direction is governed by the interfacial thermal conductances G_A, G_B, the heat capacities C_1, C_2, and C_3 of the different layers, and their out-of-plane thermal conductivities $\kappa_{\perp,1}$, $\kappa_{\perp,2}$, and $\kappa_{\perp,3}$. (b) Schematic of a MaSTR thermometry setup, where a sample is excited by pump pulses through an objective from one side, and interrogated by probe pulses through an objective from the other side. Both pump and probe pulses typically originate from the same laser, to ensure synchronization, and a delay line ensures variable delay between pump and probe pulses. The detection scheme either uses a photodetector or a spectrometer to measure reflected or back-scattered light, respectively.

We propose two types of optical probes that are particularly suited for MaSTR thermometry. The first option is to probe resonantly a temperature-sensitive mode, such as excitons in TMDs (as described in the STT section) [42, 43], plasmon resonances in metallic systems [44, 45], Mie resonances in dielectric nanoparticles [46, 47], or phonon-polaritons [48]. An increase in the lattice temperature will generate a broadening and/or a shift of the resonance [42, 43, 45, 46], which leads to a heat-dependent reflectance change at a frequency that is specifically related to a given material. The second option is to use the Raman response of the material(s). This relies on the temperature-dependent change in spectral position and/or amplitude of phonon modes of the material(s). Another option is to use the ratio of the anti-Stokes and Stokes intensity [49, 50]. Both suggested probes provide a material-specific response, thus enabling independent tracking of the temperature of different layers in a multi-layer stack. In the case of 2D materials, this allows for achieving the ultimate resolution in the out-of-plane direction, down to the atomic limit. As described in the STT section, it is important to verify that an increase in reflection is linear with an increase in pump fluence, to ensure that a change in reflection accurately describes a change in temperature.

The proposed MaSTR thermometry technique has in common with TDTR that it uses a transducer and pump and probe pulses. The main difference is that instead of inferring the temperature of the material(s) of interest indirectly through the temperature dynamics of the transducer, it obtains the temperature dynamics of the material(s) directly and with material specificity. The advantages are that more complex structures can be studied, and, under some conditions, thermal transport properties follow directly from the obtained dynamics. In the case of using exciton modes as temperature probe, the technique has similarities with STT, with the difference that the attention now lies on out-of-plane transport. In the case of using the Raman signal as probe, it has similarities with Raman thermometry.

3.2. Implementation of a material-selective time-resolved thermometry setup

Figure 3(b) presents a sketch of a possible implementation of MaSTR thermometry, where the temperature is probed by Raman spectroscopy or via reflectance changes. The pump pulses may be modulated before they reach the sample from the transducer side, in order to improve sensitivity and/or to optimize the amount of heat accumulation (see section 2.4). Ideally, the pump wavelength and power should be such that it leads to maximum absorption by the transducer and minimum absorption by the underlying layer(s). The constraints on the probe beam depend directly on the chosen type of temperature probe. When probing resonances directly through reflection measurements, the main choice is the wavelength to use, which should be close to the resonance. When probing phonon resonances through Raman measurements, the probe wavelength can be fixed, but it is important for the probe pulses to have a spectral width that is narrow enough to resolve sharp Raman features. In practice, this typically means that probe pulses need to be stretched in time to a duration of several ps [51]. The reflected or back-scattered light is then sent to a photodiode connected to a lock-in amplifier to measure the

temperature-induced reflectance change, or to a confocal module and a spectrometer for the acquisition of Raman spectra as a function of the pump-probe time delay, respectively.

3.3. Finite element simulation of the heat dynamics

We now use an Al/MoS_2/SiO_2 stack as an example system to demonstrate the utility of MaSTR thermometry, by tuning several thermal transport parameters and numerically simulating their effect on the time-dependent temperature of MoS_2. This is the temperature that will be probed through either its temperature-dependent reflection around the exciton or one of its Raman modes. We choose SiO_2 as the substrate, because it is one of the most common substrate materials, and Al as the metallic transducer, because of its rapid carrier thermalization [52–54]. The simulation consists of a finite element model [55], where each layer of the stack is divided into thinner sub-layers to generate a one-dimensional mesh, whose thickness defines the spatial resolution of the simulation in the out-of-plane direction. The temperature dynamics of each individual finite element is governed by two transport parameters [56]: an interfacial heat contribution, characterized by the TBC G between two adjacent materials [16, 57], and a conductive heat contribution based on Fourier's heat diffusion inside a given material and characterized by the out-of-plane heat conductivity $\kappa_\perp$ [58]. More details about the simulation are available in [59], and the corresponding code is openly accessible via [60].

In our Al/MoS_2/SiO_2 sample, we calculate the temperature of each MoS_2 layer as a single finite element for different delay times Δt, with the SiO_2 temperature fixed at 300 K, acting as a perfect heat sink. The simulation takes the pump-induced heating of the electrons in the Al transducer to be instantaneous, since this is orders of magnitude faster than the heat transfer across the sample [56], and lets a pump pulse excite the sample every 12.8 ns, which corresponds to a laser source with a 78 MHz repetition rate. We simulate the heat dynamics of the full system over 100 pump pulses, to reach a (quasi-)steady state in the heat accumulation regime [36] (as mentioned in section 2.4). Finally, we compute the average temperature dynamics of the MoS_2 flake after the last pulse, since this corresponds to the dynamics that would be measured in an experiment. Figure 4 displays the results of our simulations for two different thickness regimes for the MoS_2 layer: the thin layer regime and the thick layer regime.

3.4. The thin layer regime

First, we focus on the thin layer regime, represented by a 10 nm thick MoS_2 layer (16 monolayers). In figure 4(a), we show the simulated time-resolved temperature change ΔT of the MoS_2 layer. In this simulation, the TBC between MoS_2 and the substrate G_B is fixed to 15 $MWm^{-2}K^{-1}$, based on reported values for MoS_2/SiO_2 interfaces [61–63]. The TBC between Al and MoS_2 G_A is varied from 1 to 1000 $MWm^{-2}K^{-1}$. Similarly, figure 4(b) presents simulated dynamics with a fixed $G_A = 50$ $MWm^{-2}K^{-1}$, corresponding to previously measured TBC of Al/MoS_2 interfaces [7, 38], and G_B varies between 1 and 1000 $MWm^{-2}K^{-1}$. In the two cases, both the heating and the cooling of the MoS_2 flake becomes faster for increasing TBC, as expected. All simulated temperature dynamics can be described by the combination of a rising and a decaying exponential function. This leads to the rise and decay times of the MoS_2 layer as shown in figure 4(c). Below, we will show that from these timescales, we can directly obtain the TBCs G_A and G_B.

In the thin-layer regime, the temperature dynamics of the MoS_2 layer are dominated by the interfaces rather than by heat conduction in the MoS_2 layer. This is because the interfaces are more resistive to heat transport than transport within this thin layer. This means that the thermal conductivity $\kappa_{\perp,2}$ does not affect the obtained temperature dynamics, which we confirm in our simulation. We can then assume that the temperature in the MoS_2 layer is uniform and use a simple three-temperature model [64], which we use to connect the obtain timescales directly to TBCs. To this end, we use the equivalent circuit shown in figure S1 and described in Supplementary section S1. The resulting timescales are:

$$\tau_{\text{rise}} = \frac{h_2 C_2}{G_A + G_B} \tag{4}$$

$$\tau_{\text{decay}} = \frac{h_1 C_1 (G_A + G_B)}{G_A G_B}. \tag{5}$$

We plot calculated values of τ_{rise} and τ_{decay} as a function of G_A and G_B in figure 4(c), and find an excellent agreement with the obtained rise and decay times from our finite element simulations. Knowing the thicknesses and heat capacities of the used materials, one can then use the combined equations (4) and (5) to obtain G_A and G_B directly from the measured rise and decay times from a MaSTR thermometry experiment.

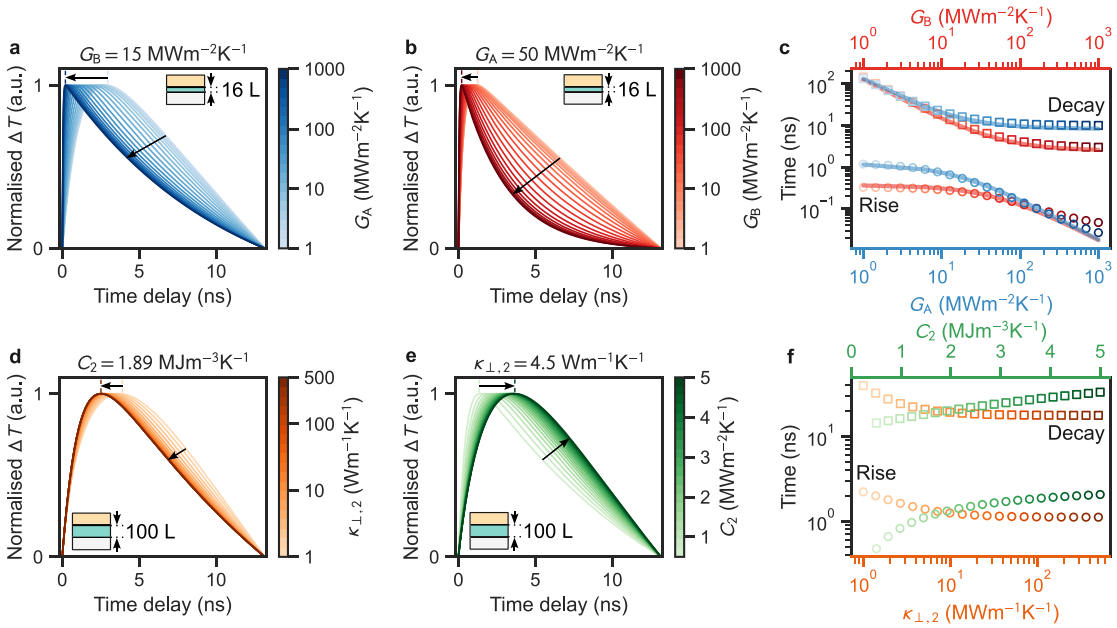

Figure 4. Simulated temperature dynamics for the example of an Al/MoS_2/SiO_2 sample. (a) Simulated temperature dynamics of the MoS_2 layer in a 50 nm-Al/16 L-MoS_2/SiO_2 sample as a function of the TBC of the first interface G_A. The TBC of the second interface is fixed as $G_B = 15$ MWm^{-2}K^{-1}, based on previously reported values for MoS_2/SiO_2 interfaces [61–63]. (b) Simulated temperature dynamics of the MoS_2 layer in a 50 nm-Al/16 L-MoS_2/SiO_2 sample as a function of G_B, with $G_A = 50$ MWm^{-2}K^{-1}, based on previously reported values for Al/MoS_2 interfaces [7, 38]. (c) Rise time (circles) and decay time (squares) from panels a and b. The continuous lines give the values predicted by a simple 3-temperature model. (d), (e) Simulated temperature dynamics of the MoS_2 layer in a 50 nm-Al/100 L-MoS_2/SiO_2 sample as a function of C_2 (d) and $\kappa_{\perp,2}$ (e). (f) Rise time (circles) and decay time (squares) from panels d and e.

3.5. Thicker flakes and more complex structures

Beyond the thin layer limit, the thermal resistance due to the out-of-plane heat conductivity $\kappa_{\perp,2}$ cannot be ignored anymore. To get an idea of its influence on the measured temperature dynamics, we run our finite element simulation on a 63 nm thick MoS_2 flake (100 monolayers) for $\kappa_{\perp,2}$ varying between 1 and 500 Wm^{-1}K^{-1}. From now on, we fix $G_A = 50$ MWm^{-2}K^{-1} and $G_B = 15$ MWm^{-2}K^{-1}, as reference TBC values for Al/MoS_2 and MoS_2/SiO_2 interfaces [7, 38, 61–63]. The results are shown in figure 4(d) and highlight how an increased conductivity results in faster dynamics. The obtained rise and decay time are shown in orange in figure 4(f) and show a similar effect of $\kappa_{\perp,2}$ on both the rise and decay time, resulting in a slower/faster heat dynamics. For completeness, figure 4(e) and the green points in figure 4(f) present simulations results as a function of the heat capacity. As expected, an increased heat capacity results in longer timescales.

3.6. Prospects and limitations of MaSTR thermometry

We believe that MaSTR thermometry is a promising approach to study heat transport in the out-of-plane direction. According to our finite element simulations, it provides complementary information to TDTR with additional benefits. In particular, in the thin-film limit, the rise and decay dynamics are directly related to thermal transport properties, which means that no numerical model is needed. Moreover, this technique provides the ability to selectively probe a composite system with material selectivity, which allows one to follow in time and space how heat travels through the different materials. In the case of 2D materials, this means sub-nanometer vertical precision can—in principle—be achieved. Whereas this has been achieved using electrical heaters and steady-state Raman scattering, MaSTR thermometry utilizes a time-resolved, all-optical approach, thereby enabling access to temporal resolution. Furthermore, the technique can be extended to perform beam-offset MaSTR thermometry experiments, by laterally offsetting the spatial offset between pump and probe beams, which are controlled by separate objectives. This would allow acquiring information on the in-plane diffusion of a given layer, in analogy to beam-offset TDTR experiments [65]. This technique also offers new ways to look at deviations from the three-temperature model, e.g. due to non-diffusive heat transport. This could, for example, manifest itself as oscillations or sign changes in the obtained signal, such as in TTG experiments [14]. Finally, even for a material that cannot be probed directly, it should be possible to estimate the out-of-plane thermal conductivity of this material by using it as a spacer between the transducer and a thinner

'temperature sensing' layer. The heat dynamics of the sensing layer would then get delayed due to the time needed for the heat to travel through the spacer layer, which is the material of interest.

For the interpretation of experimental results obtained with MaSTR thermometry—especially in cases where the thin-film limit does not apply—we expect that numerical models will be needed to extract thermal transport parameters. For this, as in TDTR experiments, sensitivity analysis will likely be essential [26]. MaSTR thermometry relies on the specificity of the optical response of a given material. In this regard, using a Raman probe is more universal than probing a temperature-sensitive exciton or plasmon mode, for example, and it can give simultaneous access to the responses of different materials. However, the latter approach has the advantage of a larger temperature sensitivity. For example, relying on the anti-Stokes to Stokes intensity ratio to measure temperature changes requires reaching local temperature differences on the order of tens of Kelvin at least, thus requiring high pump powers and long integration times [50, 66]. Despite these challenges, the technique of MaSTR thermometry can become an important addition to the toolbox of optothermal techniques aimed at understanding (nanoscale) heat transport.

4. Summary

We have presented two time-resolved, all-optical approaches for probing thermal transport in thin films. One approach, STT, extracts in-plane thermal transport from the spatial broadening of temperature profiles, while the MaSTR thermometry method probes out-of-plane heat transport by monitoring temperature dynamics within individual films. We have detailed both the experimental setups and the associated numerical methods for extracting thermal properties. These techniques provide a contact-free, high-resolution framework for studying in-plane and out-of-plane heat flow, and their applicability extends beyond two-dimensional materials to a wide range of nanoscale and multilayer systems. We anticipate that ongoing research will increasingly leverage these methods to explore non-diffusive transport regimes, including quasi-ballistic and hydrodynamic heat flow. The ability to resolve thermal dynamics with submicrometer spatial precision opens new opportunities for understanding fundamental phonon scattering processes, heat propagation at nanoscopic length scales, and thermal transport across atomic-layer interfaces, ultimately providing input to guide the thermal design of advanced materials and nanoscale devices.

Acknowledgments

K J T acknowledges funding from Spanish MCIN/AEI project PID2022- 142730NB-I00 'HYDROPTO'. ICN2 was supported by the Severo Ochoa program from Spanish MINECO Grant No. SEV-2017-0706.

Data availability statement

All data that support the findings of this study are included within the article (and any supplementary files).

Supplementary analysis 1 available at https://doi.org/10.1088/2515-7639/aea027/data1.

Author contributions

Loïc Moczko 0000-0002-2765-3357
Formal analysis (equal), Investigation (lead), Methodology (lead), Software (equal), Writing – original draft (lead)

Sebin Varghese
Investigation (lead), Methodology (lead), Software (equal), Visualization (equal), Writing – original draft (lead)

Nupur V Sontakkey
Investigation (lead), Methodology (lead), Writing – review & editing (supporting)

René J A Bruikman 0000-0003-2407-631X
Software (lead), Writing – review & editing (supporting)

Bas van Dijck 0009-0008-2439-8910
Investigation (supporting), Methodology (supporting), Writing – review & editing (equal)

Max van Hemert 0009-0005-4791-2204
Investigation (supporting), Methodology (supporting), Writing – review & editing (supporting)

David Saleta Reig
Investigation (supporting), Methodology (supporting), Writing – review & editing (equal)

Hugh Ramsden
Methodology (supporting), Writing – review & editing (equal)

Bohai Liu
Methodology (supporting), Writing – review & editing (supporting)

References

[1] Pop E, Sinha S and Goodson K E 2006 Heat generation and transport in nanometer-scale transistors *Proc. IEEE* **94** 1587–601
[2] Dhumal A R, Kulkarni A P and Ambhore N H 2023 A comprehensive review on thermal management of electronic devices *J. Eng. Appl. Sci.* **70** 140
[3] Zhang X and Zhao Li-D 2015 Thermoelectric materials: energy conversion between heat and electricity *J. Materiomics* **1** 92–105
[4] Cahill D G *et al* 2014 Nanoscale thermal transport. ii. 2003–2012 *Appl. Phys. Rev.* **1** 011305
[5] Casimir H B G 1938 Note on the conduction of heat in crystals *Physica* **5** 495–500
[6] Lee J, Lim J and Yang P 2015 Ballistic phonon transport in holey silicon *Nano Lett.* **15** 3273–9
[7] Sood A, Xiong F, Chen S, Cheaito R, Lian F, Asheghi M, Cui Y, Donadio D, Goodson K E and Pop E 2019 Quasi-ballistic thermal transport across Mos_2 thin films *Nano Lett.* **19** 2434–42
[8] Anufriev R, Gluchko S, Volz S and Nomura M 2018 Quasi-ballistic heat conduction due to Lévy phonon flights in silicon nanowires *ACS Nano* **12** 11928–35
[9] Alajlouni S, Beardo A, Sendra L, Ziabari A, Bafaluy J, Camacho J, Yi Xuan F X A and Shakouri A 2021 Geometrical quasi-ballistic effects on thermal transport in nanostructured devices *Nano Res.* **14** 945–52
[10] Lane C T, Fairbank H A and Fairbank W M 1947 Second sound in liquid helium ii *Phys. Rev.* **71** 600
[11] Narayanamurti V and Dynes R C 1972 Observation of second sound in bismuth *Phys. Rev. Lett.* **28** 1461
[12] Jackson H E, Walker C T and McNelly T F 1970 Second sound in NaF *Phys. Rev. Lett.* **25** 26
[13] Koreeda A, Takano R and Saikan S 2007 Second sound in $SrTio_3$ *Phys. Rev. Lett.* **99** 265502
[14] Huberman S, Duncan R A, Chen K, Song B, Chiloyan V, Ding Z, Maznev A A, Chen G and Nelson K A 2019 Observation of second sound in graphite at temperatures above 100 k *Science* **364** 375–9
[15] Beardo A, López-Suárez M, Pérez L A, Sendra L, Alonso M I, Melis C, Bafaluy J, Camacho J, Colombo L, Rurali R *et al* 2021 Observation of second sound in a rapidly varying temperature field in Ge *Sci. Adv.* **7** eabg4677
[16] Persson B N J, Volokitin A I and Ueba H 2011 Phononic heat transfer across an interface: thermal boundary resistance *J. Phys.: Condens. Matter* **23** 045009
[17] Yamane T, Katayama S-ichiro and Todoki M 1996 Analysis of ac temperature wave during the measurement of thermal diffusivity of two-layered platelike samples *J. Appl. Phys.* **80** 2019–26
[18] Cahill D G 1990 Thermal conductivity measurement from 30 to 750 k: the 3ω method *Rev. Sci. Instrum.* **61** 802–8
[19] Kim P, Shi Li, Majumdar A and McEuen P L 2001 Thermal transport measurements of individual multiwalled nanotubes *Phys. Rev. Lett.* **87** 215502
[20] Cahill D G, Ford W K, Goodson K E, Mahan G D, Majumdar A, Maris H J, Merlin R and Phillpot S R 2003 Nanoscale thermal transport *J. Appl. Phys.* **93** 793–818
[21] Allain A, Kang J, Banerjee K and Kis A 2015 Electrical contacts to two-dimensional semiconductors *Nat. Mater.* **14** 1195–205
[22] Reparaz J S, Chávez-Angel E, Wagner M R, Graczykowski B, Gomis-Bresco J, Alzina F and Torres C M S 2014 A novel contactless technique for thermal field mapping and thermal conductivity determination: two-laser raman thermometry *Rev. Sci. Instrum.* **85** 034901
[23] Kirsch D J, Martin J, Warzoha R, McLean M, Windover D and Takeuchi I 2024 An instrumentation guide to measuring thermal conductivity using frequency domain thermoreflectance (FDTR) *Rev. Sci. Instrum.* **95** 103006
[24] Paddock C A and Eesley G L 1986 Transient thermoreflectance from thin metal films *J. Appl. Phys.* **60** 285–90
[25] Cahill D G *et al* 2004 Analysis of heat flow in layered structures for time-domain thermoreflectance *Rev. Sci. Instrum.* **75** 5119
[26] Jiang P, Qian X and Yang R 2018 Tutorial: time-domain thermoreflectance (TDTR) for thermal property characterization of bulk and thin film materials *J. Appl. Phys.* **124** 161103
[27] Graebner J E 1995 Measurement of thermal diffusivity by optical excitation and infrared detection of a transient thermal grating *Rev. Sci. Instrum.* **66** 3903–6
[28] Maznev A A, Nelson K A and Rogers J A 1998 Optical heterodyne detection of laser-induced gratings *Opt. Lett.* **23** 1319–21
[29] Vazquez G D B, Morganti G L G, Block A, van Hulst N F, Liebel M and Tielrooij K-J 2024 Spatiotemporal microscopy: shining light on transport phenomena *Adv. Electron. Mater.* **10** 2300584
[30] Delor M, Weaver H L, QinQin Y and Ginsberg N S 2020 Imaging material functionality through three-dimensional nanoscale tracking of energy flow *Nat. Mater.* **19** 56–62
[31] Block A, Liebel M, Yu R, Spector M, Sivan Y, de Abajo F J G and van Hulst N F 2019 Tracking ultrafast hot-electron diffusion in space and time by ultrafast thermomodulation microscopy *Sci. Adv.* **5** eaav8965
[32] Block A, Renwen Y, Ieng-Wai U, Varghese S, Liebel M, van Hulst N F, Fan S, Tielrooij K-J and Sivan Y 2023 Observation of negative effective thermal diffusion in gold films *ACS Photonics* **10** 1150–8
[33] Weaver H L, Went C M, Wong J, Jasrasaria D, Rabani E, Atwater H A and Ginsberg N S 2023 Detecting, distinguishing and spatiotemporally tracking photogenerated charge and heat at the nanoscale *ACS Nano* **17** 19011–21

[34] Utterback J K, Sood A, Coropceanu I, Guzelturk B, Talapin D V, Lindenberg A M and Ginsberg N S 2021 Nanoscale disorder generates subdiffusive heat transport in self-assembled nanocrystal films *Nano Lett.* **21** 3540–7
[35] De Bellis F, Feldman M, Delbono I, Royer S, Prado Y, Cruguel H, Lacaze E, Lhuillier E and Utterback J K 2025 Simultaneous electronic and thermal signatures in pump–probe spectroscopy of semiconductor nanocrystal films *Nano Lett.* **25** 7317–25
[36] Varghese S *et al* 2023 A pre-time-zero spatiotemporal microscopy technique for the ultrasensitive determination of the thermal diffusivity of thin films *Rev. Sci. Instrum.* **94** 034903
[37] Schmidt A J, Chen X and Chen G 2008 Pulse accumulation, radial heat conduction and anisotropic thermal conductivity in pump-probe transient thermoreflectance *Rev. Sci. Instrum.* **79** 114902
[38] Jiang P, Qian X, Xiaokun G and Yang R 2017 Probing anisotropic thermal conductivity of transition metal dichalcogenides MX_2 (M = Mo, W and X = S, Se) using time-domain thermoreflectance *Adv. Mater.* **29** 1701068
[39] Chester M 1963 Second sound in solids *Phys. Rev.* **131** 2013–5
[40] Varghese S *et al* 2026 Controllable hydro-thermoelastic heat transport in ultrathin semiconductors at room temperature *Nat. Phys.* 22 1057–63
[41] Chen D *et al* 2025 Anisotropic thermal transport in quasi-2D Ruddlesden-Popper hybrid perovskite superlattices *Phys. Rev. X* **15** 041054
[42] Selig M, Berghäuser G, Raja A, Nagler P, Schüller C, Heinz T F, Korn T, Chernikov A, Malic E and Knorr A 2016 Excitonic linewidth and coherence lifetime in monolayer transition metal dichalcogenides *Nat. Commun.* **7** 13279
[43] Cadiz F *et al* 2017 Excitonic linewidth approaching the homogeneous limit in MoS_2-based van der waals heterostructures *Phys. Rev. X* **7** 021026
[44] Leung P T, Hider M H and Sanchez E J 1996 Surface-enhanced Raman scattering at elevated temperatures *Phys. Rev. B* **53** 12659–62
[45] Himstedt R, Baabe D, Wesemann C, Bessel P, Hinrichs D, Schlosser A, Bigall N C and Dorfs D 2021 Temperature-sensitive localized surface plasmon resonance of α-nis nanoparticles *J. Phys. Chem. C* **125** 26635–44
[46] Fiedler S, Monin L, Sugimoto H, Fujii M, Albrecht W and Polman A 2025 Nanoscale heat flow and thermometry in laser-heated resonant silicon Mie nanospheres probed with spatially resolved cathodoluminescence spectroscopy *ACS Photonics* **12** 5668–74
[47] Assadillayev A, Hinamoto T, Fujii M, Sugimoto H and Raza S 2021 Thermal near-field tuning of silicon Mie nanoparticles *Nanophotonics* **10** 4161–9
[48] Chen Y, Pacheco M A S, Salihoglu H and Xianfan X 2024 Greatly enhanced radiative transfer enabled by hyperbolic phonon polaritons in α-MoO_3 *Adv. Funct. Mater.* **34** 2403719
[49] Sandell S, Chávez-Ángel E, Sachat A E, Jianying H, Torres C M S and Maire J 2020 Thermoreflectance techniques and Raman thermometry for thermal property characterization of nanostructures *J. Appl. Phys.* **128** 131101
[50] Peter Y Y and Cardona M 2005 *Fundamentals of Semiconductors: Physics and Materials Properties* 3rd edn (Springer)
[51] Versteeg R B, Zhu J, Padmanabhan P, Boguschewski C, German R, Goedecke M, Becker P and van Loosdrecht P H M 2018 A tunable time-resolved spontaneous Raman spectroscopy setup for probing ultrafast collective excitation and quasiparticle dynamics in quantum materials *Struct. Dyn.* **5** 044301
[52] Yu A V, Palatnik L S and Pugachev A T 1976 Investigation of the thermal properties of thin aluminum *J. Exp. Theor. Phys.* **43** 1171
[53] Wang Y, Park J Y, Koh Y K and Cahill D G 2010 Thermoreflectance of metal transducers for time-domain thermoreflectance *J. Appl. Phys.* **108** 043507
[54] Wilson R B, Apgar B A, Martin L W and Cahill D G 2012 Thermoreflectance of metal transducers for optical pump-probe studies of thermal properties *Opt. Express* **20** 28829–38
[55] George P 2024 *Finite Element Formulation for Heat Transfer* (Springer)
[56] Giri A, Gaskins J T, Donovan B F, Szwejkowski C, Warzoha R J, Rodriguez M A, Ihlefeld J and Hopkins P E 2015 Mechanisms of nonequilibrium electron-phonon coupling and thermal conductance at interfaces *J. Appl. Phys.* **117** 105105
[57] Ong Z-Y, Cai Y and Zhang G 2016 Theory of substrate-directed heat dissipation for single-layer graphene and other two-dimensional crystals *Phys. Rev. B* **94** 165427
[58] Fourier J B J 1878 *The Analytical Theory of Heat* (The University Press)
[59] Bruikman R J A 2024 Towards time-resolved Raman thermometry for out-of-plane heat transport in transition metal dichalogenides *Master's Thesis* Eindhoven University of Technology
[60] Available at: https://github.com/lmoczko-tue/LRT-simulation
[61] Yalon E *et al* 2017 Temperature-dependent thermal boundary conductance of monolayer mos2 by Raman thermometry *ACS Appl. Mater. Interfaces* **9** 43013–20
[62] Suryavanshi S V, Gabourie A J, Farimani A B and Pop E 2019 Thermal boundary conductance of two-dimensional mos2 interfaces *J. Appl. Phys.* **126** 055107
[63] Gabourie A J, Köroğlu Çağıl and Pop E 2022 Substrate-dependence of monolayer mos2 thermal conductivity and thermal boundary conductance *J. Appl. Phys.* **131** 195103
[64] Sergei I A, Kapeliovich B L and Perelman T L 1974 Electron emission from metal surfaces exposed to ultrashort laser pulses *J. Exp. Theor. Phys.* **39** 375–7
[65] Rodin D and Yee S K 2017 Simultaneous measurement of in-plane and through-plane thermal conductivity using beam-offset frequency domain thermoreflectance *Rev. Sci. Instrum.* **88** 014902
[66] Shen X, Fan A, Wang H, Zhang X and Wang X 2020 Raman-based nanoscale thermal transport characterization: a critical review *Int. J. Heat Mass Transfer* **154** 119751